

Serveur Académique Lausannois SERVAL serval.unil.ch

Author Manuscript

Faculty of Biology and Medicine Publication

This paper has been peer-reviewed but does not include the final publisher proof-corrections or journal pagination.

Published in final edited form as:

Title: An introduction to model-independent diffusion magnetic resonance imaging.

Authors: Van AT, Granziera C, Bammer R

Journal: Topics in magnetic resonance imaging : TMRI

Year: 2010 Dec

Volume: 21

Issue: 6

Pages: 339-54

DOI: 10.1097/RMR.0b013e31823e6303

In the absence of a copyright statement, users should assume that standard copyright protection applies, unless the article contains an explicit statement to the contrary. In case of doubt, contact the journal publisher to verify the copyright status of an article.



Published in final edited form as:

Top Magn Reson Imaging. 2010 December ; 21(6): 339–354. doi:10.1097/RMR.0b013e31823e6303.

An Introduction to Model-Independent Diffusion MRI

Anh Tu Van¹, Cristina Granziera², and Roland Bammer¹

¹ Department of Radiology, Stanford University, Stanford, CA, U.S.A. ² Department of Neurology, Centre Hospitalier Universitaire Vaudois and University of Lausanne, Lausanne, Switzerland

Abstract

Q-space based techniques such as diffusion spectrum imaging, q-ball imaging, and their variations have been used extensively in research for their desired capability to delineate complex neuronal architectures such as multiple fiber crossings in each of the image voxels. The purpose of this paper is to provide an introduction to the q-space formalism and the principles of basic q-space techniques together with the discussion on the advantages as well as challenges in translating these techniques into clinical environment. A review of the currently used q-space-based protocols in clinical research is also provided.

1. Introduction

The possibility to map and study human brain connections, pathways, and networks has long been a very attractive field of research. Initially driven by basic neuroscience research, this field of study enjoys increasing popularity in the clinical space. Nowadays, magnetic resonance imaging (MRI) techniques help one to map cerebral functional and structural connectivity *in vivo* and non-invasively. Here, measures of structural connectivity – obtained by diffusion MRI experiments – complement functional connectivity typically measured by means of blood oxygenation level dependent (BOLD) contrast. Diffusion imaging builds upon the fact that spins in biological tissue are not static. Driven by thermal energy they instead move constantly along random paths. The average region a spin covers during a given observation interval is associated with the diffusion coefficient.

From its early experiments describing the measurement of this physical property via NMR by Hahn (Hahn 1950) and later by Carr and Purcell (Carr and Purcell 1954) until now, diffusion MRI has made major strides. The most commonly used diffusion MRI technique is diffusion-weighted imaging (DWI). DWI allows one to map the apparent diffusion coefficient (ADC) of protons in tissue. In this context, the ADC is an average index of how freely water can move within a voxel (i.e. averaged across all tissue structures and compartments within the voxel) and hence the term “apparent.” In its simplest form, a diffusion-weighted image can be formed with diffusion-encoding gradients played out only along one of the principal axes (e.g., x, y, or z) or a combination thereof. Early on, Moseley et al. (Moseley, Cohen et al. 1990) found that diffusion in (feline) neural tissue depends on the orientation of white matter relative to the externally applied diffusion-encoding gradients. In white matter, they found that the diffusion coefficient is higher when measured along fiber bundles, than perpendicular to these fibers. Thus, it has been suggested to perform DWI along at least the three principal axes and average these three images to mitigate false positive findings from white matter diffusion anisotropy that could otherwise be misinterpreted as diffusion reductions due to cytotoxic edema (Moseley, Cohen et al. 1990). Simple as it is, DWI has been the key method for diagnosing acute stroke as well as other brain pathologies including, but not limiting to, tumors, brain infections, and Creutzfeldt-Jakob disease.

A more complex diffusion MRI technique, first introduced by Basser et al. (Basser, Mattiello et al. 1994), is diffusion tensor imaging (DTI). In addition to ADCs, DTI also provides directionality information of the diffusion process in the structure of interest. On the basis of diffusion anisotropy, this directionality information has spun off an entirely new field of research that focuses on non-invasively tracing white matter tracts (a.k.a. tractography or fiber tracking). Tractography in turn allows one to interrogate and mapping structural connections between different regions of the brain as well as helps clinicians to improve their understanding of the invasiveness and mass effects of neoplasms and facilitate presurgical planning. In addition, a large number of studies have suggested the use of metrics of diffusion anisotropy to reveal regions of abnormal underlying brain tissue otherwise occult to the skilled human observer. The validity of these metrics – often used within the context of voxel-based morphometry (VBM) for group or per-patient comparison studies – is not yet without controversy.

Early after the discovery of DTI-based tractography, it became evident that – despite of its many benefits – DTI suffered from important limitations that also carried over to tractography. The veracity of the reconstruction of fiber trajectories was insufficient particularly when complex fiber architectures were interrogated (Wiegell, Larsson et al. 2000; Alexander, Hasan et al. 2001; Alexander, Barker et al. 2002; Frank 2002; Tuch, Reese et al. 2002). Although diffusion imaging is sensitive to microscopic diffusive motion, what is accessible to imaging is the net effect from the entire voxel. Here, DTI has very limited capabilities to resolve multiple fiber bundle orientations inside an imaging voxel. A major shortcoming of DTI is the use of a single tensor to model complex diffusion processes occurring within a voxel. Obviously, biologic tissues are usually heterogeneous, and a single diffusion tensor is not able to distinguish complex fiber trajectories that are, for example, crossing, kissing, branching, or merging within a voxel or a cluster of voxels.

However, this rather complex fiber architecture is more or less the standard in the normal brain (Behrens, Berg et al. 2007). Crossing fibers, kissing fibers, or similar patterns are essential features of superficial and deep brain structures (i.e. cerebral and cerebellar cortex, corona radiata, and pontine decussation, Figure 1). As a matter of fact, crossing/branching/merging fibers are also considered to be one of the major hallmarks of cerebral plasticity mechanisms, concomitant or consequent to brain neurological and psychiatric diseases, such as stroke, epilepsy, traumatic brain injury, schizophrenia, autism, and so forth (Sutula 2002; Dancause, Barbay et al. 2005; Thompson, Gibson et al. 2006; Chapleau, Larimore et al. 2009; Zalesky, Fornito et al. 2011). In addition, these phenomena characterize normal and abnormal developmental processes (Huttenlocher 2002) as well as task learning and training (Imfeld, Oechslin et al. 2009).

Most of the studies that provide important insights on the mechanisms underlying cerebral plasticity have been performed in the experimental field (Chopp, Li et al. 2008; Jiang, Zhang et al. 2010; Jiang, Zhang et al. 2010). However, the mismatch between the organization of rodents and primate brain with the one of the human brain represents a major limitation to draw direct conclusions. Moreover, it is well known that neural circuits are shaped by genes and environmental co-factors/stimuli during early phases of brain development (Hubel and Wiesel 1970). Therefore, each individual is characterized by its unique organization of brain connections and networks (“connectome”, (Sporns 2011)). In this context, the capability of non-invasively depicting and subsequently deciphering the complexity of the human cerebral connectivity, pathways, and network could allow one to understand individual mechanisms of cerebral plasticity. This in turn could eventually afford more targeted rehabilitation or training programs, as well as drug therapy.

The challenge to disentangle the multiple fiber directions contained within a single voxel volume drives most of the recent developments of diffusion MRI techniques towards seeking alternative algorithms, models, or encoding schemes with the overarching goal to garner more detailed information about the underlying orientation of white matter fibers.

This manuscript aims to provide an overview of an encoding scheme, more specifically q-space encoding (Callaghan 1991), that can provide a model-free diffusion description of the diffusion process in complex environment such as biological tissues. As compared to model-based approach, such as DTI, this model-free description of the diffusion process has the potential to yield more accurate structure and orientation information of the imaged object regardless of its complexity. The paper focuses on two representatives of the q-space encoding technique: Diffusion Spectrum Imaging (DSI, (Wedeen, Hagmann et al. 2005) and q-ball imaging (Tuch 2004). Unlike DTI, DSI and q-ball MRI require the application of much stronger diffusion-encoding gradients and much larger numbers of encoding steps. Hence, these methods lead to lengthy acquisition times and had limited the applicability of these techniques to dedicated MRI centers and research applications. Despite the technical challenges, the implementation of dedicated protocols (Granziera C., Benner T. et al. 2008; Kuo, Chen et al. 2008; Granziera, Daducci A. et al. 2011), commercially available pulse sequences (Krueger 2008) as well as the widespread availability of high field system 3 Tesla systems, powerful magnetic gradient systems, and multi-channel head coils renders it now possible to use these techniques for clinical applications.

The remainder of this paper is organized as follows: Section 2 discusses the source of directional information detected by diffusion imaging; Section 3 introduces the q-space formalism, which is the most general, model-free representation of diffusion imaging signal; Section 4 describes the two most basic q-space based imaging techniques (i.e. diffusion spectrum imaging and q-ball imaging); Section 4 discusses the usefulness as well as the challenges of q-space techniques from a clinical perspective and describes several DSI/q-ball protocols currently used for clinical research; Section 5 concludes the paper with summary of the methods and discusses their benefits as well as limitations for clinical use.

2. Diffusion Imaging Is The Measurement of The Average Displacement of Molecules within a Voxel

Traditional structural imaging techniques, such as T1-weighted or T2-weighted imaging, provide only a 2D or 3D representation of the anatomy studied. In other words, each of the voxels in a 3D T1-, T2-weighted image is represented by a single number (a.k.a. a scalar) that is determined by the T1 or T2 relaxation property of the underlying tissue at the corresponding voxel's location. However, information about the organization of tissue within a voxel or its structural orientation (if any) is not available. Diffusion imaging techniques provide access to this microscopic organization and directionality information by “following” the randomly moving protons while they “probe” the tissue. Since the motion of protons is 3D, ideally an additional 3D encoding (on top of the 3D image encoding) is needed for each voxel to fully characterize the diffusive motion, which renders diffusion imaging a six-dimensional imaging technique (see Figure 2).

To simplify the illustration, the voxel of interest (red box in the left panel of Figure 2) is assumed to consist of only two tubular structures with different orientations (right panel of Figure 2). As the molecules move randomly (as shown by the green and the blue trajectories) within these tubes (as well as outside), their motion — restricted by the tubes' boundaries (for example myelin sheets) — reflects the structure and also the orientation of the tubes. More specifically assuming the orientation of the tubes in Figure 2 is known, if we measure the ADC (the index of how freely water can move) in the direction perpendicular to

the main axes of the tubes, due to the restriction of the tubes' boundaries, the obtained value should be much smaller than if we measure in the direction parallel to the main axes of the tubes. On the other hand, if we do not know the orientation of the tubes but instead know ADCs in every direction, we can guess with high precision the orientation of the tubes, i.e. parallel to the directions with the largest measured ADCs.

If one can assume that the measured ADCs of a voxel in different directions (ADC profile) form a regular shape, such as a sphere or an ellipsoid, the number of measurements needed to deduce the ADC value in every direction and hence the information about the structure as well as the orientation of tissues within a voxel will be reduced.

In fact, for unrestricted diffusion such as diffusion of water in a "big" container where water molecules can diffuse in any direction with equal probability, it is valid to assume that the ADC profile approximates a sphere. In this case, only one measurement (for the estimation of the radius of the sphere) is needed to fully characterize the ADC profile. Ignoring the complexity of restricted diffusion, diffusion tensor imaging (DTI) extends this spherical ADC profile model to ellipsoidal ADC profile model (Figure 3) for the case of restricted diffusion. The short radii of the ADC ellipsoid represent the direction that diffusion is most restricted while the long radius corresponds to the direction that diffusion is least restricted. Mathematically, the assumption of either spherical or ellipsoidal ADC profile comes from the Gaussian diffusion process assumption.

With this ellipsoidal ADC profile assumption, for each voxel, DTI attempts to fit a 3D ellipsoid, which is the geometry representation of a rank-2 tensor (hence the name diffusion tensor imaging), to ADC values measured along at least six (non-collinear) directions in 3D space (three measurements for estimating the three radii and three for estimating the direction of the main axis of the ellipsoid). Thus, DTI is a scan-time-efficient method for estimating the directionality information in the imaged structures.

Soon after DTI was discovered, it was realized however that the ellipsoidal ADC profile is an oversimplified assumption for the diffusive motion of molecules in biological tissue, especially within voxels that demonstrate more complex organizations of fibers or where more than one dominant axonal bundle existed within a voxel (Alexander, Hasan et al. 2001; Alexander, Barker et al. 2002; Frank 2002). Examples of the ADC profile of molecules within a voxel that has two and three fibers passing through are given in Figure 4. These ADC profiles clearly deviate from a 3D ellipsoid, rendering the DTI assumption invalid. It appears evident that attempts to fit 3D ellipsoids to such data would lead to inaccurate results with large fit errors.

3. Beyond DTI

The above deviations from DTI's ellipsoid model motivated the development of a wide variety of more complex models and algorithms for extracting more information that can help resolving the complex organization of fibers within a voxel.

The most natural extension from the DTI's single ellipsoid model is the multi-ellipsoid model, or formally multi-tensor model. As its name implies, the multi-tensor model fits multiple ellipsoids (tensors) to the measured displacement data and therefore can detect the existence of multiple fiber orientation within a voxel.

However, since the number of parameters needed estimating grows relatively fast with the number of tensors used, the estimation problem becomes unstable at high number of tensors, requiring further constraints for stabilization (Tuch, Reese et al. 2002; Behrens, Woolrich et al. 2003; Alexander and Barker 2005; Hoseney, Williams et al. 2005; Behrens, Berg et al.

2007). Furthermore, the multi-tensor model loses accuracy when the number of distinct fiber populations in the underlying voxel differs from the number of tensors used in the model (Jones 2011). Ideally, one would want to use the appropriate model for each voxel of interest, i.e., use a one-tensor model for voxels with one fiber population, a two-tensor model for those with two fiber populations, and so on. Therefore, the choice of model is of critical importance. Notice that even though the proper choice of the number of tensors used improves the estimated fiber orientations, the accuracy of the estimation is still compromised by the fact that the diffusion process in restricted environment such as in biological tissues is much more complex than just a superposition of a series of Gaussian diffusion processes.

In another effort to go beyond DTI, Alexander et al. (Alexander, Barker et al. 2002) proposed the spherical harmonic decomposition of the ADC profile. Spherical harmonics are the angular portion of a set of solutions of Laplace's equation. Each of the function is well defined by two integers: l , called the degree, and m , called the order, where $-l \leq m \leq l$. Examples of spherical harmonics of different degrees and orders are given in Figure 5.

An arbitrary 3D spherical structure can be modeled through the weighted summation of a limited set of spherical harmonics, which are 3D basis structures. Conversely, spherical harmonic decomposition is telling one the weights for each of these 3D basis structures, which when combined would closely resemble the arbitrary 3D object.

In this spherical decomposition method, the ADC profile of a voxel is modeled as a linear combination of the spherical harmonics of up to a certain order. Since the spherical harmonics are known, the only parameters to estimate are the coefficients of the linear combination. Similar to the case of the multi-tensor model, the spherical harmonic order used to decompose the ADC profiles should change from voxel to voxel depending on the underlying structure. The reason is that higher-order terms might only represent noise added to the data during the image acquisition process (Alexander, Barker et al. 2002). The spherical harmonic order used to decompose the ADC profile in each of the voxel is determined through a statistical test. Starting from the lowest order, the procedure iterates by increasing the order of the spherical harmonic used until this increase does not change (as judged from the statistical test results) the description of the estimated ADC profile.

The advantage of the spherical harmonic decomposition is that any ADC profile can be fully described. However, the extraction of ADC profile from the measured data requires again the unrealistic assumption of Gaussian diffusion process in complex environments such as biological tissues, compromising the accuracy of the model in estimating the orientations of fibers. By measuring the ADC along a particular diffusion-encoding direction one already assumes an underlying Gaussian diffusion process, as e^{-bADC} is the result of a spin displacement probability distribution that is Gaussian.

Model-based approaches for estimation of fiber orientations within a voxel such as the aforementioned multi-tensor and spherical harmonic decomposition have the common advantage of requiring only a small number of measurements. However, any model, regardless of how sophisticated, assumes some special scenario that might not always be valid, leading to limitations in accuracy and generality in estimating fiber orientations within a voxel with arbitrary underlying tissue structures. Hence, to be able to accurately estimate the fiber direction in a voxel with arbitrary fiber configuration, model-free approaches are needed. In the following section, the framework upon which most of the model-free approaches are built will be discussed.

3. Q-Space

For all the model-based approaches, theoretically the number of diffusion measurements needed equals the number of parameters for the model. For example, a two-tensor (or two-ellipsoid model) would require 12 independent measurements (six measurements to describe each ellipsoid.) When no model is used, estimation of the fiber orientation requires the characterization of a fully 3D diffusion process. Therefore, a 3D measurement of the diffusion-driven displacement of water molecules in the voxel of interest is needed. The signal generated by the 3D diffusion measurement of each voxel is called the q-space signal (Callaghan 1991).

Figure 6 shows how q-space signal can be obtained with a typical spin-echo acquisition. In Figure 6, the two shaded trapezoids are the two diffusion-encoding gradient pulses. Do note that the q-space approach differs theoretically from a classic Stejskal-Tanner diffusion-weighted spin-echo sequence (Stejskal and Tanner 1965) by using very short, but extremely strong, diffusion-encoding gradients. This is to minimize the influence of spin displacement while these gradients are played. Also as will be discussed later, different from DTI acquisitions, q-space signal is acquired with varying diffusion-encoding-gradient amplitudes or spacing.

Consider an arbitrary voxel within which spins (or equivalently water molecules) move around continuously and explore the underlying tissues. When the first shaded trapezoid is applied, a “label” is put on all of the spins, marking its location. As “label” we are basically putting on an extra phase to the spin (remember the magnetization has magnitude and phase). This extra phase that is put on top of the complex magnetization depends on spin location, gradient strength, and gradient duration. For example, for a spin at location r (mm) from the center of the voxel and with the gradient strength (the height of the trapezoid) of G_d (mT/m), and the gradient duration δ (ms)(Figure 6), the value of this phase is $\gamma G_d \delta r$ radian, where γ is the gyromagnetic ratio and $\gamma = 2\pi \times 42.576$ MHz/T.

After the labeling procedure, the molecules continue to move around. At a later time, in a similar fashion, the second trapezoid is played out which puts a second label on each of the spins. The second label's phase depends on the new location and again on strength and duration of the diffusion-encoding gradient. Assuming that the spin considered previously now moves to the new location at $(r + R)$, in a similar fashion as before, the magnetization of this spin gets an additional phase of $\gamma G_d \delta (r + R)$ radian. Taking into account the effect of the 180° that reverses the sign of the phase introduced by the first diffusion gradient, the total phase that both diffusion gradients induced on the spin at the end of the second diffusion gradient is $-\gamma G_d \delta r + \gamma G_d \delta (r + R) = \gamma G_d \delta R$, resulting in a complex magnetization of $\exp(j\gamma G_d \delta R)$ (assuming that the magnitude of the magnetization of a single spin is 1) which is independent of its starting position.

The ensemble-averaged signal of a voxel with a certain diffusion gradient configuration (i.e., a certain set of values G_d , δ , and Δ) is the sum of the complex magnetizations of all the spins within that voxel, which in this case is:

$$E(G_d, \Delta) = \sum_R n_R \exp(j\gamma G_d \delta R), \quad (1)$$

where n_R is the number of spins in the voxel that experience a diffusion-driven relative displacement of R during the time interval Δ , and the sum is taken over all possible relative displacements experienced by different spins within that voxel. If we define N_{spin} to be the

total number of spins within the voxel of interest, the portion of spins within that voxel that experienced a diffusion-driven displacement of R over the time Δ will be

$$P(R, \Delta) = \frac{n_R}{N_{spin}}. \quad (2)$$

Formally, $P(R, \Delta)$ is called the displacement distribution function of spins or probability density function (PDF) of spin displacement within the voxel of interest. In other words P tells the likelihood of spins to diffuse a distance R within an interval Δ along the direction the diffusion-encoding gradient is played out. Notice that since R represents the displacement in 3D, $P(R, \Delta)$ captures the 3D diffusion process of spins within the voxel.

From Equation (2), n_R can be expressed as

$$n_R = N_{spin} P(R, \Delta). \quad (3)$$

By replacing Equation (3) into Equation (1), the relationship between the q-space signal and the displacement distribution function of spins within a voxel is

$$E(G_d, \Delta) = \sum_R N_{spin} P(R, \Delta) \exp(j\gamma G_d \delta R). \quad (4)$$

Define a new parameter q :

$$q = \frac{1}{2\pi} \gamma G_d \delta, \quad (5)$$

Equation (4) can be rewritten as

$$E(q, \Delta) = \sum_R N_{spin} P(R, \Delta) \exp(j2\pi q R). \quad (6)$$

For the reader it is important to realize that the relationship between the acquired q-space signal ($E(q, \Delta)$) and the displacement distribution function ($P(R, \Delta)$) in Equation (6) resembles the relationship between k-space and image space in conventional MRI, i.e. the Fourier relationship. In other words, the Fourier transform of $P(R, \Delta)$ yields the spectrum (i.e. weights) of the wave functions (q-value) that comprise P and hence explains the term diffusion spectrum imaging. The set of wave functions is also called q-space. By acquiring the q-space signal $E(q, \Delta)$ and taking the Fourier transform, $P(R, \Delta)$ can be derived, giving a model-free description of the diffusion process within the voxel of interest.

Individual points in q-space can be acquired by choosing arbitrary values of G_d or δ to set a desired q-value. Obviously, to traverse q-space in 3D, different values for G_d along the x-, y-, or z-dimension need to be picked. To fully encode q-space of dimension N_{qx} , N_{qy} , and N_{qz} a total of $N_{qx} \cdot N_{qy} \cdot N_{qz}$ q values are needed. The resolve ever-finer details of P , ever-higher wave functions need to be acquired. That is, N_{qx} , N_{qy} , and N_{qz} need to be large, otherwise only a blurred version of the true P can be acquired. (Remember this is similar to acquiring a larger area of k-space in conventional MR imaging). Similarly, the maximum spatial extent R of the true P that can be acquired without causing aliasing in the

reconstructed P depends on how dense q -space is sampled and according to the Nyquist criterion yields $\Delta q = 1/R_{\max}$. (Remember this is similar to the k -space sampling density that is required to sample a given FOV without aliasing). That said, Δq obviously depends – for a given observation interval Δ – on the underlying diffusion coefficient as *can be seen from the Einstein equation: $x^2 = 2 \cdot D \cdot \Delta$* .

For q -space imaging (in applications such as resolving axon diameters), diffusion has some important implication on the ability to resolve structures in it. That is, the diffusion of a particle spin makes it difficult to spatially localize it. The effective resolution of q -space imaging R_{eff} is determined by the resolution of the PDF ($1/q_{\max}$) and the root-mean-square (Einstein) displacement of the diffusing particle ($\sqrt{2D\Delta}$) (Wedeen and Dai 2011). In other words:

$$R_{\text{eff}}^2 = \frac{1}{q_{\max}^2} + 2D\Delta \quad (7)$$

By letting $t = \delta = \Delta$ and $q_{\max} = \frac{\gamma}{2\pi} G_{\max} t$, the equation above evaluates to:

$$R_{\text{eff}}^2 = \frac{4\pi^2}{(\gamma G_{\max} t)^2} + 2Dt \quad (8)$$

With a maximum diffusion gradient strength – determined by the system – and a set diffusion coefficient D – determined by the structure under interrogation, the maximum resolution that can be observed in such a setup depends on the diffusion time t . Thus,

$d(R_{\text{eff}}^2)/dt = 0$ yields that the smallest resolution, $R = \sqrt{3} \left(\frac{2\pi D}{\gamma G_{\max}} \right)^{1/3}$, is achieved with

$\Delta_{\text{opt}} = \left(\frac{4\pi^2}{\gamma^2 G_{\max}^2} D \right)^{1/3}$ and $t_{\text{opt}} = \frac{8\pi^2}{3\gamma^2 D}$. From the Equation (7) above one can see that for short Δ , the minimum achievable resolution is determined by the q -value one can observe by increasing Δ for a given maximum gradient amplitude. However, the minimum achievable resolution worsens as Δ increases beyond a particular duration when the long diffusion time makes the resolution dependent on the diffusion (Einstein term). Thus, there is an optimal Δ_{opt} for each maximum gradient strength (and D) that determines resolution. One can therefore conclude that the only way one can improve resolution is by stronger gradients.

As mentioned at the beginning of the section, the q -space signal is obtained by performing a 3D diffusion-driven displacement measurement. One can change the direction of the displacement measurement by changing the labeling direction, which is the direction along which the diffusion-encoding gradient pair (the shaded trapezoids in Figure 6) is played out. In turn, the direction along which the diffusion-encoding gradients are played out can be achieved by adjusting the gradient strength on each of the three axes, G_x , G_y , and G_z , individually. An illustration of the measurement direction adjustment for three different measurement directions is given in Figure 7.

Due to the complexity and heterogeneous nature of biological tissues, it is expected that molecules within such tissues experience different levels of restriction that modulate the spin displacements differently. Therefore, another important aspect of measuring the average displacement is the precision level of the labeling, meaning the length scale (tens of micrometer, micrometer, or nanometer...) on which the label can record the location of the molecule. As we have shown in the previous paragraph, higher labeling precision is desired

because of its capability to capture smaller displacements. The length precision of the labeling can be adjusted by changing the total amplitude of the diffusion-encoding gradients on three principal gradient channels (i.e. the overall magnitude of the effective 3D gradient [vector]). The greater the magnitude, the finer details in the 3D displacement can be resolved. However, revealing ever-finer details of the spin displacement comes at the price of lower signal amplitude or lower signal-to-noise ratio (SNR).

In summary, the q-space is the 3D space with coordinates (q_x, q_y, q_z) defined by the diffusion-encoding gradients on the three channels $G_x, G_y,$ and G_z . Here, q and G on each axis relate to each other by: $q = \frac{1}{2\delta} \gamma G \delta$. The q-space signal, $E(q, \Delta)$, at a particular coordinate point in q-space, (q_x, q_y, q_z) , is the diffusion-weighted spin-echo MR-signal that is obtained when the diffusion-encoding gradients are applied corresponding to these q-space coordinate points. The q-space signal at this coordinate point has its magnitude modulated by both the average displacement of the molecules within a voxel and the amplitude of the diffusion-encoding gradients. Because of its dependence on the average displacement of molecules within a voxel, the q-space signal provides an indirect measurement of the organization of tissues in the voxel of interest. Similar to getting from k-space to an MR image, a 3D Fourier Transformation of q-space data, yields the 3D probability distribution function (PDF) for spin displacement.

Figure 8 gives an illustration of how the q-space signal is acquired at different voxels within an image. For each of the diffusion-encoding steps (q-values), a diffusion-weighted image is obtained. Here, the q-space signal for a voxel is the collection of the magnitudes of that voxel in all the diffusion-weighted images acquired with different q-values. Hence, to sample q-space of size $N_{qx}, N_{qy},$ and N_{qz} a total of $N_{qx} \times N_{qy} \times N_{qz}$ diffusion-weighted scans is required. The large number of images that are required to produce q-space information of reasonable resolution is hence another challenge to perform q-space imaging in a clinical setup. Rapid imaging methods, such as single-shot echo-planar-imaging (EPI), and scans to sample q-space more efficiently are therefore critically important. Depending on the q-space imaging techniques (see next paragraph), the sampling of q-space values and the post processing algorithms that are used to obtain and extract the tissue organization information can differ. Here, a large effort went into making q-space imaging more efficient and less time demanding, to facilitate clinical adoption.

4. Q-Space Imaging Techniques

With the rapid evolution of MR diffusion imaging methods, the literature now contains a wide variety of q-space based techniques, which allow one to provide a more precise and efficient description of complex tissue structures. In this section, we do not attempt to provide a complete review of the existing techniques, but rather aim to introduce the basic concepts behind the most popular and established techniques together with their benefits and limitations.

a) Diffusion Spectrum Imaging

Diffusion spectrum imaging (DSI) (Wedeen, Hagmann et al. 2005) collects q-space signal, $E(q, \Delta)$, with values of q traversing the 3D q-space. An example of 3D q-space traverse following 3D Cartesian grid is shown in Figure 9. In essence, DSI is the extension of the single-voxel q-space NMR (Callaghan 1991) to multi-voxel application with the clinical magnet and gradient systems.

For each voxel, the q-space signal – or equivalently the set of all $E(q, \Delta)$ values – is 3D Fourier transformed and yields the 3D likelihood function for a spin to be displaced along a certain direction within the observation interval Δ . As mentioned before this 3D likelihood

function is usually called the displacement distribution or also the probability density function (PDF) for spin displacement. A two-dimensional illustration of the procedure of estimating the PDF from the q-space signal for a single voxel is given in Figure 10 (adopted from Jones' book, Chapter 27 (Jones 2011)). The left panel shows the q-space signal ($E(q, \Delta)$) for every possible pair of q-values (q_x, q_y) (since we are considering a 2D example, each of the q-value has only two coordinates). Only at the white dots one is measuring q-values. The colors encode the amplitude of the q-space signal where red is the highest and blue is the lowest. All q-space signals at the white dots are processed (by the two-dimensional "FFT" operation) to achieve the values of the PDF ($P(R, \Delta)$) at the red dot locations. On the right panel, each of the red dots, specified by the pair (x, y), represents the reconstructed spin displacement, while the regions between the sample points show the continuous representation of the displacement (i.e. infinite q-space sampling). Here, the colors at location (x, y) encode the relative likelihood $P(R, \Delta)$ of molecules within the voxel of interest to be displacement from the origin to the support point (x, y) within the diffusion time Δ , where $R^2 = x^2 + y^2$. The color red represents the highest and blue the lowest likelihood.

From the displacement distribution of the molecules within each voxel, various information about the tissue microstructure in that voxel can potentially be extracted. For fiber tracking or connectivity mapping applications the most commonly used information is the fiber orientation distribution function (Tuch 2004; Wedeen, Hagmann et al. 2005).

Basically, the fiber orientation distribution function (ODF) is a metric of how likely fibers within a voxel orient in certain directions. Fiber tracking can be done by following the directions indicating the highest orientation likelihood, i.e. the high value regions of the ODFs, from one voxel to another.

Since spins move more freely along the fibers than perpendicular to them, it is common practice to assume the probability of spin displacement along a certain direction as a surrogate for the orientation probability of fibers. However, caution needs to be exercised and one needs to be aware that also the ODF represents an ensemble average for each voxel and not individual fibers.

The probability of spin displacement along a certain direction (or directional displacement probability) can be easily estimated from the displacement distribution as described in Figure 11. Consider an arbitrary direction on the PDF map shown in Figure 11, for example either of the directions pointed out by the green arrows. Then, the probability that spins move along either of those directions equals the sum of PDF values along the corresponding green arrow, weighted by the square of their distance to the origin:

$$\text{ODF}(\mathbf{u}) = \sum_R R^2 P_{\mathbf{u}}(R, \Delta) dR \quad (9)$$

In Equation (9), \mathbf{u} refers to the directions of the green lines in Figure 11, $P_{\mathbf{u}}(R, \Delta)$ is the PDF value at distance R from the origin along the \mathbf{u} direction, and dR is the spatial distance between the two consecutive sampled points of $P_{\mathbf{u}}(R, \Delta)$.

For a discretely sampled PDF, such as with DSI, the directional displacement probability is computed at multiple directions and then interpolated to get an estimation of a continuous ODF (blue line on the right panel of Figure 11). Alternatively, one could resample the Cartesian PDF values along the spokes for which the ODF is desired.

Figure 12 shows the ODFs in the area of corpus callosum (Figure 12b) and the mid brain (Figure 12c) derived from a DSI acquisition (acquired by the Advanced Biomedical MRI

Lab at National Taiwan University Hospital and is available for download at: dsi-studio.labsolver.com/download-images). The maximum b-value used was 4,000 s/mm² obtained with diffusion timing parameters $\Delta/\delta = 80/35$ ms, number of q-space points was 203. DSI data were processed using the DSI studio package available at: dsi-studio.labsolver.com.

Recall that in DSI, the average displacement of molecules is estimated directly from the measured data without any assumption on the structure of the underlying tissue as well as the form of the displacement. It is therefore a model-free approach. Hence, the achieved average displacement or the orientation distribution function (ODF) is more accurate and reveals more information about the configuration of the tissue in complex cases than model-based approaches, such as DTI.

DSI offers a complete description of the random motion of molecules within a voxel. Therefore, DSI has the potential of providing much more information about the organization of the tissues within the voxel of interest than just the preferred direction of the tissues. As mentioned before, the rich information provided by DSI comes at an expensive cost: excessive total acquisition time. To accurately reconstruct the 3D displacement distribution (right panel of Figure 10) and hence the ODF, DSI has to sample the q -space signal on a fine-enough 3D Cartesian grid and with sampling far enough out in q -space to cover fine details of the PDF. Here, we have seen that similar analogies to k -space and corresponding features in MR images can be used. That is, central portions of q -space provide coarse features of the PDF, whereas peripheral regions of q -space determine fine details of the PDF. The further out in q -space sample points are acquired the more details of the PDF can be recovered. The sparser q -space is sampled the smaller the FOV of the PDF that can be sampled without aliasing. This needs to be considered especially with longer diffusion times, Δ , or for species with higher overall diffusivity, which tend to have a broader PDF.

Overall, the criteria for choosing the q -space sampling distance and extent depend on the anticipated spatial extent of the PDF and the resolution (i.e. level of detail) at which one wants to resolve the distribution. This is similar to the choice to the acquisition matrix in a conventional MRI acquisition (e.g. 64×64 vs. 256×256 matrix). The former affords rapid scanning at the cost of low spatial resolution. Currently, the prime factor determining DSI studies is the scan time needed for all measurements. For a DSI study of human white matter, investigators report acquisition protocols that typically require around 500 measurements (q -values). Such protocol leads to a total scan time of about 30 minutes (Wedeen, Hagmann et al. 2005). However, with recent advancements in acquisition techniques, DSI acquisition has become more clinically feasible (Breuer, Blaimer et al. 2005; Feinberg, Moeller et al. 2010; Setsompop, Cohen-Adad et al. 2010; Menzel, Sperl et al. 2011; Van, O'Halloran et al. 2011).

The theory of DSI is based upon the assumption that the diffusion-encoding gradients (shaded trapezoid in Figure 6) have extremely short duration, to guarantee that motion occurs between the labeling pulses but not during the time when those gradients are played out (Callaghan 1991). In practice, this assumption is not true due to hardware limitations of clinical MRI systems. The resulting effect is blurring of the displacement distribution $P(R, \Delta)$ and the derived ODF (Mitra and Halperin 1995). Therefore, interpretation of the DSI results has to be carried out with care, taking into account the blurring effects.

b) Q-Ball Imaging

To overcome the time consuming disadvantage of DSI, while maintaining the capability of probing the tissue structure without any modeling, the q-ball imaging technique was introduced (Tuch 2004). Instead of sampling q -space on a complete 3D q -space trajectory,

such as a 3D Cartesian grid, the q-ball technique traverses q-space only on a sphere with large enough diameter (Figure 13), so that the average displacement of molecules can be captured with high enough precision. Although the q-ball technique still requires quite a large number of q values (diffusion encoding directions), this number is considerable smaller than the full-fledged DSI approach, resulting in much shorter scan time while still maintaining the capability to resolve complex tissue structure, such as multiple crossing fibers.

It has been proven mathematically that the q-ball imaging technique can give an approximation of the ODF simply by taking the Funk-Radon transform (FRT) of the spherically sampled q-space signal (Tuch 2004). Imagine that the q-ball sampling points are all distributed on the surface of the globe, then the approximate value of the ODF (i.e. the result of the FRT) along the direction that connects the south and the north pole is the sum of all the measured q-space signal on the equator (Hagmann, Jonasson et al. 2006). In general, to compute the approximate value of the ODF in an arbitrary direction, take the sum of all q-space signal on the “new equator” perpendicular to the direction under consideration.

To get an intuition on why the FRT of the q-space signal can give an estimation of the ODF, let us consider Figure 14. Examples of the q-ball signals on two different “equators” (E_1 and E_2) are shown in panel (a) of Figure 14. Panel (b) of Figure 14 gives the positions of the two q-ball equators with respect to the imaged structure, in this case a single fiber. The directions that are perpendicular to the equators are also shown (D_1 is perpendicular to E_1 and D_2 is perpendicular to E_2).

Recall that the magnitude of a voxel (or equivalently the q-space signal of that voxel) in a diffusion-weighted experiment is higher if the diffusion-encoding direction (q value) is along the more diffusion-restricted direction of that voxel. Therefore, if the voxel in consideration contains a fiber like that in panel (b) of Figure 14, the measured q-ball signal is the highest in the directions that are perpendicular to the fiber and decreases as the directions change to parallel to the fiber. Therefore, the sum of the q-ball signals measured on the equator E_1 , which is perpendicular to the fiber, is higher than on the equator E_2 , which is not perpendicular to the fiber, as shown in panel (c) of Figure 14.

Inversely, with the cylinder fiber (panel (b) of Figure 14) that we are considering, it is more likely that the fiber orients perpendicular to the plane that the diffusion is the most restricted (or the diffusion-weighted (q-space) signal is the highest). Therefore, in Figure 14, E_1 and E_2 gives an estimation of the fiber orientation probability in the direction D_1 and D_2 , respectively. Panel (d) of Figure 14 gives the ODF of the fiber in panel (b) of Figure 14, overlaid with the two directions D_1 and D_2 .

Although the above intuition is given for the case of a single cylinder fiber, Tuch has proven mathematically that irrespective of the geometry of the underlying structure, the FRT of the spherically sampled q-space signal gives an estimation of the ODF (Tuch 2004). Other method for estimating the ODF from q-ball measurement was also proposed (Hess, Mukherjee et al. 2006).

Figure 15 shows the obtained ODFs in a region of interest (marked by the yellow box on the right panel of Figure 15) from a q-ball acquisition with 150 non-colinear directions at a b-value of 2,500 s/mm^2 . DSI studio package (dsi-studio.labsolver.org) was used to process the data. Crossing fibers were reasonably detected with the estimated ODFs.

Regarding scan time, q-ball imaging is much more manageable than DSI because of a much smaller number of q-space sample points one has to acquire while still maintaining the

capability to account for complex tissue structure, such as multiple crossing fibers. However, due to the difference in sampling and reconstruction, it is worth to notice that the q-ball-derived ODF is different from the DSI-derived ODF. Mathematically, the relationship between the q-ball-derived ODF and the PDF (spin displacement distribution) is:

$$\text{ODF}^{\text{q-ball}}(\mathbf{u}) = \sum_R P_{\mathbf{u}}(R, \Delta) J_0(|q|R) dR \quad (10)$$

Equation (10) is different from Equation (9), which describes the relationship between DSI-derived ODF, in two ways. First, the summation in Equation (10) is not weighted by the square of the distance, R^2 . Second, the summation in Equation (10) is instead weighted by the function $J_0(|q|R)$, which is a sinc-shaped function (Tuch 2004). This differences results in an estimated ODF with less distinctive primary maxima. So, overall it is very important to report which method was used to generate the ODF.

The function $J_0(|q|R)$ more and more resembles a delta dirac function, $\delta(R)$, and therefore has less effects on the computation of the ODF when the radius of the sampled q-ball increases. Hence, improvement of the q-ball-derived ODF can be obtained by increasing the radius of the q-ball. However, the increased radius (equivalent to increased b-value) results in noisier diffusion-weighted images, or equivalently noisier q-space signals, that might introduce other errors to the estimation of the ODFs. There is no established method for choosing the optimal radius (as well as the number of sampled points/directions) of q-ball experiments. Most of the published q-ball experiments used a b-value in the range 2,500 to 4,000 s/mm² with more than 250 directions (Tuch, Reese et al. 2003; Tuch 2004; Kuo, Chen et al. 2008).

Furthermore, unlike DSI, there is no direct intuitive relationship between the q-ball-estimated ODF and the actual ODF; therefore, further validation of the accuracy of q-ball imaging is required.

4. Discussion

a) DSI/ q-ball, where would it be useful: a clinician's perspective

The initial applications of q-ball and DSI techniques gave astonishing results in depicting the anatomy of cerebral pathways (Tuch 2004; Granziera C., Hadjikhani N. et al. 2011), cerebellar cortical structures and circuits (Granziera, Schmahmann et al. 2009), as well as brain networks (Hagmann, Cammoun et al. 2008). Moreover, recent studies showed that DSI could visualize the anatomical networks underlying functional resting state activity in the brain (Honey, Sporns et al. 2009). Very few studies applied q-ball and DSI to patients, thus far (Granziera C., Benner T. et al. 2008; Granziera C., Benner T. et al. 2008; Granziera, Daducci A. et al. 2011; Lo, Soong et al. 2011). This is due mostly to the lack of clinical q-ball or DSI protocols and time constraints, as well as a lack of user-friendly post-processing packages (when compared to DTI).

A major question to the clinician is still what is the real gain of DSI/q-ball imaging sequences compared to the more traditional DTI that would justify the extra effort? – A very interesting study by Gigandet et al. (Gigandet X., Kober T. et al. 2010) compared two DSI acquisition schemes (with 258 directions-DSIq5 and with 129 directions and 2 averages - DSIq4), one q-ball study (257 directions), and one DTI scan (65 directions and 4 averages). For this study the same scan time was held constant (i.e., 26 minutes). Similarly, the acquisition parameters and the number of averages for the four studies were chosen so that the same signal to noise ratio (SNR) could be achieved. Tractography was performed using

the *Trackvis* software and a connectivity matrix was obtained as described by (Hagmann, Cammoun et al. 2008). This study showed that a DTI scan might be an adequate solution when (1) investigating large anatomical pathways, (2) when scan time is a crucial factor, and (3) when dealing with uncooperative patients. However, this study also clearly pointed out that some precautions have to be taken when considering fiber tracts running through large fiber crossing areas, such as the *arcuate fasciculus* or the *superior longitudinal fasciculus*. In that case, already a DSIq4 scan (acquisition time of ~12 minutes) should provide enough contrast to better identify major fiber bundles of the brain; even more so when investigating neighboring association fibers (in the 60-90mm range). Here, a DSI scan with 258 or more encoding gradients is preferable.

Therefore, it seems clear that there is indeed an advantage in anatomical accuracy when performing DSI/q-ball in specific brain regions and structures, especially when DTI studies run the risk of suggesting fiber tracts that are mostly equivocal or entirely on error.

At present, it remains however an open question, whether DSI or q-ball techniques could offer a substantial contribution to clinical research and practice. A theoretical gain of these methods over existing DTI would concern the study of mechanisms of brain networks and their plasticity changes that could provide one new diagnostic, therapeutical, and prognostic markers of disease. Moreover, they could also give substantial contribution in monitoring brain development.

Nevertheless, the application of DSI and q-ball to patients is still a challenge for a number of reasons. The first reason is the reproducibility of these techniques. Reproducibility has been studied comprehensively for diffusion tensor imaging (Heiervang, Behrens et al. 2006), but only few studies consider this topic for DSI or q-ball imaging. Reproducible q-ball and DSI results are possible but the caveat is that a number of sources of variability need to be considered and minimized (i.e., image acquisition settings, image segmentation, registration, ODF reconstruction and tractography algorithms). Recent studies on q-ball and DSI reproducibility are focused on the analysis of specific connectivity tracts (Granziera C., Benner T. et al. 2008; Nezamzadeh, Wedeen et al. 2010), selected brain structures (Schmahmann, Pandya et al. 2007; Granziera, Schmahmann et al. 2009), and single networks (i.e. motor network (Daducci A., Gigandet X. et al. 2010; Granziera, Daducci A. et al. 2011)). Therefore, current studies are lacking aim at understanding the global variability of these techniques and more comprehensive investigations are warranted in adequate cohorts of subjects.

The second reason is that quantitative metrics derived from DSI and q-ball images are needed. If for DTI, the fractional anisotropy (FA) metric is an overall accepted quantitative measure (Basser and Pierpaoli 1996), for q-ball and DSI there is still substantial work to be done to develop an accepted metric that – if at all possible – contracts information into a single number like FA. Tuch (Tuch 2004) has proposed an equivalent of fractional anisotropy for q-ball and DSI named generalized fractional anisotropy. However, only one DSI study of post-stroke recovery applied it, thus far (Granziera, Daducci A. et al. 2011). Other possible measures are the number of fiber trajectories per region of interest (such as tract density metrics) or various other metrics of fiber density. However, they all suffer from the limitation that the metric is intrinsically tied to the tractography algorithm (and seeds) used and thus biased.

The third reason addresses the need for standardized processing methods in order to be able to relate results from different settings and centers. Post-processing methods to be applied to q-ball and DSI results are still lengthy and need to be performed off-line. Some reconstruction software packages are nowadays freely available (www.trackvis.org;

dsi-studio.labsolver.org; www.nitrc.org/projects/mrtrix) but tractography reconstruction need to be performed with specific parameters selected on the base of the acquisition protocol used and this renders these tools good instruments for clinical research but not for clinical practice. Clear guidelines and a consensus on postprocessing parameters are critically needed.

The fourth reason is that it appears that the actual performance of the most commonly applied tractography algorithms depends on the patients' age (Daducci A., Gigandet X. et al. 2010), which renders the actual application of these techniques feasible in clinical research where age-matched control groups could be selected but again not for routine clinical practice.

The fifth reason is that due to the longer scan time, those techniques are more prone to motions artifacts and are very demanding on the scanner hardware. Many methods have been developed to perform motion correction during the image acquisition process (Aksoy, Forman et al. 2011; Benner, van der Kouwe et al. 2011). However, despite its obvious benefits neither retrospective nor prospective motion correction methods have yet become widely available.

To gain SNR and speed, the spatial resolution of DSI scans is lower than general DTI or DWI scans. Hence, limited spatial resolution is another tradeoff. In other words, one gains better resolution of fibers within a voxel, but on the other hand larger voxel size makes it harder to tease apart fiber structures. Considerable research has still to be done here to identify whether or not it is better to have better spatial resolution or better resolution of the PDF.

Lastly, despite the broader availability of 3T systems and multi-channel coils, the experiments with 10,000 and more diffusion-encoding steps with b-values as high as the suggested optimal value of 18,000 s/mm² (Wedeen and Dai 2011) for a single subject scan represent highest demands on the gradient duty cycles and overall system stability in DSI and q-ball experiments. Here gradient heating, scanner drift, peripheral nerve stimulation, and increased levels of ghosting/misregistration need to be kept in mind.

b) Clinical research protocols

To date, very few clinical applications of q-ball and DSI have been published (Granziera C., Benner T. et al. 2008; Rose, Pannek K. et al. 2010; Granziera, Daducci A. et al. 2011). This is mainly because DSI and q-ball has been suffering from the major drawback of lengthy scan times, due to the targeted high b-values. In fact, there is also a lack of recommendations for optimal Δ , maximum q-values, and q-space sampling density.

A certain improvement in scan time can be obtained with the help of a system with stronger gradients, by use of parallel imaging, and higher signal-to-noise ratios from multi-channel coils and higher magnetic fields. Obviously, the use of specially built head insert gradients, which are short and have smaller inner diameter would offer higher gradient strength and higher rise times. This in turn would afford very high b-values and faster readouts without considerable neurostimulation. Conversely, existing RF-coils need to fit within such coils and retrofitted with a transmit coil.

Faster acquisitions could also be achieved by reducing the spatial resolution. However, it has become evident that voxel sizes larger than approximately 2 mm³ could not provide adequate anatomical information. Another option that has been proposed recently is to perform a more efficient sampling of the q-space (Wu and Alexander 2007; Yeh, Wedeen et al. 2010). Alternatively, one could carry out a multi-slice excitation (Feinberg, Moeller et al.

2010; Setsompop, Cohen-Adad et al. 2010)) to speed up acquisition. However, also these methods come with limitations, such as exceeding the specific absorption rate (SAR) per kg tissue or larger geometric distortions. Moreover, these methods are currently in the exploratory stage and to date not ready for clinical “prime time.”

The real need of extremely high b-max values has also been questioned for q-ball and DSI experiments. In order to study this criticism, Kuo et al. (Kuo, Chen et al. 2008) compared four sampling schemes, two with high sampling number, i.e., DSI-515 and QBI-493, and two with low sampling number, i.e., DSI-203 and QBI-253, in a 3T Siemens system and concluded that the optimum maximum b-value was a tradeoff between SNR and angular resolution. Specifically on Kuo's 3T system, the optimum maximum b-value (in units of s/mm^2) were 6,500 for DSI-515, 4,000 for DSI-203, 3,000 for QBI-493 and 2,500 for QBI-253.

Based on the aforementioned thoughts, there are some DSI and q-ball imaging (QBI) protocols available that are dedicated to clinical research applications (Kuo, Chen et al. 2008; Granziera, Schmahmann et al. 2009). Specifically, these clinical protocols are implemented to find a tradeoff between an adequate SNR and an acceptable scan time for patients. Most importantly, they are substantially shorter than experimental research protocols published previously (Wedeen, Wang et al. 2008; Takahashi, Dai et al. 2011) and are normally designed to optimize the gain for the specific disease for which they were implemented.

c) Index cases

Some DSI studies have been recently performed to a number in cohorts of stroke (Granziera C., Benner T. et al. 2008; Granziera C., Benner T. et al. 2008; Granziera C., Hadjikhani N. et al. 2011) and autistic patients; another few are currently being performed in epilepsy and schizophrenia.

Concerning stroke, one pilot study compared q-ball data to DTI data in patients with stroke (Granziera C., Benner T. et al. 2008; Granziera C., Benner T. et al. 2008) and showed that q-ball performed better than DTI (with regards to tractography showing the tracts more accurately) if the analyzed tract had a complex anatomy (e.g. arcuate fascicle) or extended through regions of fiber crossing (cortico-spinal tract) (Figure 16).

In addition, very recently, DSI has been shown to be able to detect changes in the motor network of the healthy hemisphere of stroke patients up to six months after the acute event and to predict their degree of functional recovery (Figure 17, (Granziera C., Hadjikhani N. et al. 2011)).

Another promising application of DSI is to epileptic patients for pre-surgical planning. It appears in fact that DSI, better than DTI, can help to map the connections along which the epileptic discharge diffuse. An example of DSI and DTI tractography performed in a patient with a right posterior cingulate cavernoma and right anterior temporal epileptic source is shown in Figure 18.

As to DSI applied to psychiatric diseases, a recent work of Lo et al., (Lo, Soong et al. 2011) showed that DSI protocols are also tolerated by young patients affected by autism. In this study, GFA alterations were measured in long-range tracts involved in social cognition and language processing in participants with autism (cingulum, arcuate fascicle, uncinate fascicle, and callosal fiber tracts). The major findings of this study was that adolescents with autism had significantly lower mean GFA values in the three callosal fiber tracts than

control subjects and that patients did not show any asymmetry of the studied long-range connections compared to controls.

5. Conclusion

This manuscript has reviewed the techniques for resolving diffusion anisotropy from the basic DTI to the complex DSI and q-ball imaging. By considering the basic diffusion process in heterogenous tissue, such as white matter, we showed challenges and shortcomings of established methods, such as DTI and other tensor-based techniques, specifically when attempting to resolve complex tissue structure scenarios, such as the coexistence of an arbitrary number of fiber orientations within a voxel. There exist many more techniques beyond DTI for recovering multiple fiber orientations in each image voxel, the most general of which is DSI. It was the aim of this paper to raise awareness of these alternatives and highlight some of the shortcomings of DTI methods.

Based on the foundations of the diffusion process itself – without any assumptions on either the signal model or the configuration of the underlying tissues – q-space imaging or DSI possesses the unique ability to fully characterize diffusion without the need of any model assumption. Potentially, a lot of information regarding the tissue within each image voxel can be retrieved from the displacement distribution estimated from DSI.

Ong et al., in a recent work (Ong and Wehrli 2011) showed the possibility of extracting the axon diameter distribution (ADD) from the PDF estimated from DSI data. In that work, the PDF was first separated into intra- and extra-cellular components using a two-compartment model (Assaf, Blumenfeld-Katzir et al. 2008). Three further assumptions were made to facilitate the estimation of the ADD including the ADD followed a gamma distribution, the mean axon diameter approximated the full-width-half-max (FWHM) of the intra-cellular PDF, and the cross section of an axon is circular.

Until now, little success has been made in differentiating between certain types of fiber configurations such as crossing fibers vs. kissing fibers. Since the types of diffusion restriction in these scenarios (crossing vs. kissing) are different, in theory, the displacement PDFs should be different, potentially allowing the classification. The questions, of course, are how significant is the difference and what type of displacement resolution (the largest q-value) is needed to resolve the difference.

When the ODF is the only information one is interested in, q-ball imaging appears to be a more (time) efficient model-free method. Notice also that unlike DSI, there is no direct intuitive relationship between the q-ball-estimated ODF and the actual ODF, requiring further accuracy validation of q-ball method.

Both DSI ODFs and q-ball ODFs are derived relying on heuristic relationships between the displacement distribution ($P(R, \Delta)$) and the actual fiber orientation distribution (fODF) within each voxel. However, it remains unclear to what extent the estimated ODFs reflect the fODF.

Many other techniques exist in the literature attempting to extract the ODF with more complicated still heuristic relationships between $P(R, \Delta)$ and fODF such as spherical deconvolution (Anderson and Ding 2002; Tournier, Calamante et al. 2004), persistent angular structure (Jansons and Alexander 2003), diffusion orientation transform (Ozarslan, Shepherd et al. 2006), or hybrid diffusion imaging (Wu and Alexander 2007). One has to distinguish between association between diffusion measurement and fiber orientation and the use of an implicit model to characterize diffusion in a heterogenous medium (e.g. DTI).

All in all, there are no rigid criteria for evaluating and comparing the performance of different methods. The choice of the method therefore is still basing on the users' preference. A summary of the advantages and disadvantages of the three diffusion-imaging methods discussed in this paper is given in Table 1.

References

- Aksoy M, Forman C, et al. Real-time optical motion correction for diffusion tensor imaging. *Magn Reson Med*. 2011
- Alexander AL, Hasan KM, et al. Analysis of partial volume effects in diffusion-tensor MRI. *Magn Reson Med*. 2001; 45(5):770–780. [PubMed: 11323803]
- Alexander DC, Barker GJ. Optimal imaging parameters for fiber-orientation estimation in diffusion MRI. *Neuroimage*. 2005; 27(2):357–367. [PubMed: 15921931]
- Alexander DC, Barker GJ, et al. Detection and modeling of non-Gaussian apparent diffusion coefficient profiles in human brain data. *Magn Reson Med*. 2002; 48(2):331–340. [PubMed: 12210942]
- Anderson, AW.; Ding, Z. Sub-voxel measurement of fiber orientation using high angular resolution diffusion tensor imaging.. 10th International Society for Magnetic Resonance in Medicine (ISMRM) conference; Honolulu. 2002.
- Assaf Y, Blumenfeld-Katzir T, et al. AxCaliber: a method for measuring axon diameter distribution from diffusion MRI. *Magn Reson Med*. 2008; 59(6):1347–1354. [PubMed: 18506799]
- Basser PJ, Mattiello J, et al. Estimation of the effective self-diffusion tensor from the NMR spin echo. *J Magn Reson B*. 1994; 103(3):247–254. [PubMed: 8019776]
- Basser PJ, Pierpaoli C. Microstructural and physiological features of tissues elucidated by quantitative-diffusion-tensor MRI. *J Magn Reson B*. 1996; 111(3):209–219. [PubMed: 8661285]
- Behrens TE, Berg HJ, et al. Probabilistic diffusion tractography with multiple fibre orientations: What can we gain? *Neuroimage*. 2007; 34(1):144–155. [PubMed: 17070705]
- Behrens TE, Woolrich MW, et al. Characterization and propagation of uncertainty in diffusion-weighted MR imaging. *Magn Reson Med*. 2003; 50(5):1077–1088. [PubMed: 14587019]
- Benner T, van der Kouwe AJW, et al. Diffusion imaging with prospective motion correction and reacquisition. *Magn Reson Med*. 2011
- Breuer FA, Blaimer M, et al. Controlled aliasing in parallel imaging results in higher acceleration (CAIPIRINHA) for multi-slice imaging. *Magn Reson Med*. 2005; 53(3):684–691. [PubMed: 15723404]
- Callaghan, PT. Principles of nuclear magnetic resonance microscopy. Clarendon Press ; Oxford University Press; Oxford England New York: 1991.
- Carr HY, Purcell EM. Effects of Diffusion on Free Precession in Nuclear Magnetic Resonance Experiments. *Physical Review*. 1954; 94(3):630–638.
- Chapleau CA, Larimore JL, et al. Modulation of dendritic spine development and plasticity by BDNF and vesicular trafficking: fundamental roles in neurodevelopmental disorders associated with mental retardation and autism. *J Neurodev Disord*. 2009; 1(3):185–196. [PubMed: 19966931]
- Chopp M, Li Y, et al. Plasticity and remodeling of brain. *J Neurol Sci*. 2008; 265(1-2):97–101. [PubMed: 17610903]
- Daducci, A.; Gigandet, X., et al. On the reproducibility and anatomical correspondence of DSI tractography. *Human Brain Mapping*; Barcelona, Spain: 2010.
- Dancause N, Barbay S, et al. Extensive cortical rewiring after brain injury. *J Neurosci*. 2005; 25(44): 10167–10179. [PubMed: 16267224]
- Feinberg DA, Moeller S, et al. Multiplexed echo planar imaging for sub-second whole brain fMRI and fast diffusion imaging. *PLoS One*. 2010; 5(12):e15710. [PubMed: 21187930]
- Frank LR. Characterization of anisotropy in high angular resolution diffusion-weighted MRI. *Magn Reson Med*. 2002; 47(6):1083–1099. [PubMed: 12111955]

- Gigandet, X.; Kober, T., et al. A Connectome-Based Comparison of Diffusion MR Acquisition Schemes.. 19th International Society for Magnetic Resonance in Medicine (ISMRM) conference; Stockholm, Sweden. 2010.
- Granziera, C.; Daducci, A., et al. Diffusion Spectrum Imaging after stroke shows structural changes in the contra-lateral motor network correlating with functional recovery.. 19th International Society for Magnetic Resonance in Medicine (ISMRM) conference; Montreal, Canada. 2011.
- Granziera C, Schmahmann JD, et al. Diffusion Spectrum Imaging Shows the Structural Basis of Functional Cerebellar Circuits in the Human Cerebellum In Vivo. *Plos One*. 2009; 4(4)
- Granziera, C.; Benner, T., et al. A Comparison Between Diffusion Tensor Imaging and Q-Ball MRI in the Study of Post-Stroke Plasticity. 16th International Society for Magnetic Resonance in Medicine (ISMRM) conference; Toronto, Canada. 2008.
- Granziera, C.; Benner, T., et al. Monitoring post-stroke plasticity in patients with good functional recovery: A comparison between diffusion tensor and qball magnetic resonance imaging. American Academy of Neurology; Boston, MA, USA: 2008.
- Granziera C, Hadjikhani N, et al. In-vivo magnetic resonance imaging of the structural core of the Papez circuit in humans. *Neuroreport*. 2011; 22(5):227–231. [PubMed: 21346644]
- Hagmann P, Cammoun L, et al. Mapping the structural core of human cerebral cortex. *PLoS Biol*. 2008; 6(7):e159. [PubMed: 18597554]
- Hagmann P, Jonasson L, et al. Understanding diffusion MR imaging techniques: from scalar diffusion-weighted imaging to diffusion tensor imaging and beyond. *Radiographics*. 2006; 26(Suppl 1):S205–223. [PubMed: 17050517]
- Hahn EL. Spin Echoes. *Physical Review*. 1950; 80(4):580–594.
- Heiervang E, Behrens TEJ, et al. Between session reproducibility and between subject variability of diffusion MR and tractography measures. *Neuroimage*. 2006; 33(3):867–877. [PubMed: 17000119]
- Hess CP, Mukherjee P, et al. Q-ball reconstruction of multimodal fiber orientations using the spherical harmonic basis. *Magn Reson Med*. 2006; 56(1):104–117. [PubMed: 16755539]
- Honey CJ, Sporns O, et al. Predicting human resting-state functional connectivity from structural connectivity. *Proc Natl Acad Sci U S A*. 2009; 106(6):2035–2040. [PubMed: 19188601]
- Hosey T, Williams G, et al. Inference of multiple fiber orientations in high angular resolution diffusion imaging. *Magn Reson Med*. 2005; 54(6):1480–1489. [PubMed: 16265642]
- Hubel DH, Wiesel TN. The period of susceptibility to the physiological effects of unilateral eye closure in kittens. *J Physiol*. 1970; 206(2):419–436. [PubMed: 5498493]
- Huttenlocher, P. *Cerebral plasticity*. Cambridge, MA: 2002.
- Imfeld A, Oechslin MS, et al. White matter plasticity in the corticospinal tract of musicians: a diffusion tensor imaging study. *Neuroimage*. 2009; 46(3):600–607. [PubMed: 19264144]
- Jansons KM, Alexander DC. Persistent angular structure: new insights from diffusion magnetic resonance imaging data. *Inverse Problems*. 2003; 19(5):1031–1046.
- Jiang Q, Zhang ZG, et al. MRI evaluation of white matter recovery after brain injury. *Stroke*. 2010; 41(10 Suppl):S112–113. [PubMed: 20876482]
- Jiang Q, Zhang ZG, et al. MRI of stroke recovery. *Stroke*. 2010; 41(2):410–414. [PubMed: 20035069]
- Jones, DK. *Diffusion MRI : theory, methods, and applications*. Oxford University Press; Oxford: 2011.
- Krueger, G. Application guide EP2D DSI work-in-progress package for diffusion spectrum imaging in siemens. 2008.
- Kuo LW, Chen JH, et al. Optimization of diffusion spectrum imaging and q-ball imaging on clinical MRI system. *Neuroimage*. 2008; 41(1):7–18. [PubMed: 18387822]
- Lo YC, Soong WT, et al. The loss of asymmetry and reduced interhemispheric connectivity in adolescents with autism: a study using diffusion spectrum imaging tractography. *Psychiatry Res*. 2011; 192(1):60–66. [PubMed: 21377337]
- Menzel, MI.; Sperl, JL., et al. Improved sampling patterns for accelerated diffusion spectrum imaging using compressed sensing.. 19th International Society for Magnetic Resonance in Medicine (ISMRM) conference; Montreal, Canada. 2011.

- Mitra PP, Halperin BI. Effects of Finite Gradient-Pulse Widths in Pulsed-Field-Gradient Diffusion Measurements. *Journal of Magnetic Resonance Series A*. 1995; 113(1):94–101.
- Moseley ME, Cohen Y, et al. Diffusion-weighted MR imaging of anisotropic water diffusion in cat central nervous system. *Radiology*. 1990; 176(2):439–445. [PubMed: 2367658]
- Nezamzadeh M, Wedeen VJ, et al. In-vivo investigation of the human cingulum bundle using the optimization of MR diffusion spectrum imaging. *Eur J Radiol*. 2010; 75(1):e29–36. [PubMed: 19615838]
- Ong, HH.; Wehrli, FW. Assessment of axon diameter distribution in mouse spinal cord with q-space imaging.. 19th International Society for Magnetic Resonance in Medicine (ISMRM) conference; Montreal, Canada. 2011.
- Ozarslan E, Shepherd TM, et al. Resolution of complex tissue microarchitecture using the diffusion orientation transform (DOT). *Neuroimage*. 2006; 31(3):1086–1103. [PubMed: 16546404]
- Rose, S.; Pannek, K., et al. The FA Connectome: A Quantitative Strategy for Studying Neurological Disease Processes.. 18th International Society for Magnetic Resonance in Medicine (ISMRM) conference; Stockholm, Sweden. 2010.
- Schmahmann JD, Pandya DN, et al. Association fibre pathways of the brain: parallel observations from diffusion spectrum imaging and autoradiography. *Brain*. 2007; 130(Pt 3):630–653. [PubMed: 17293361]
- Setsonpop, K.; Cohen-Adad, J., et al. Improving SNR per unit time in diffusion imaging using a blipped-CAIPIRINHA simultaneous multi-slice EPI acquisition.. 18th Annual Meeting of the ISMRM; Stockholm, Sweden. 2010.
- Sporns O. The human connectome: a complex network. *Ann N Y Acad Sci*. 2011; 1224(1):109–125. [PubMed: 21251014]
- Stejskal EO, Tanner JE. Spin Diffusion Measurements: Spin Echoes in the Presence of a Time-Dependent Field Gradient. *Journal of Chemical Physics*. 1965; 42(1):288–.
- Sutula T. Seizure-Induced Axonal Sprouting: Assessing Connections Between Injury, Local Circuits, and Epileptogenesis. *Epilepsy Curr*. 2002; 2(3):86–91. [PubMed: 15309153]
- Takahashi E, Dai G, et al. Developing neocortex organization and connectivity in cats revealed by direct correlation of diffusion tractography and histology. *Cereb Cortex*. 2011; 21(1):200–211. [PubMed: 20494968]
- Thompson SN, Gibson TR, et al. Relationship of calpain-mediated proteolysis to the expression of axonal and synaptic plasticity markers following traumatic brain injury in mice. *Exp Neurol*. 2006; 201(1):253–265. [PubMed: 16814284]
- Tournier JD, Calamante F, et al. Direct estimation of the fiber orientation density function from diffusion-weighted MRI data using spherical deconvolution. *Neuroimage*. 2004; 23(3):1176–1185. [PubMed: 15528117]
- Tuch DS. Q-ball imaging. *Magn Reson Med*. 2004; 52(6):1358–1372. [PubMed: 15562495]
- Tuch DS, Reese TG, et al. High angular resolution diffusion imaging reveals intravoxel white matter fiber heterogeneity. *Magn Reson Med*. 2002; 48(4):577–582. [PubMed: 12353272]
- Tuch DS, Reese TG, et al. Diffusion MRI of complex neural architecture. *Neuron*. 2003; 40(5):885–895. [PubMed: 14659088]
- Van, AT.; O'Halloran, R., et al. Rapid diffusion spectrum imaging with partial q-space encoding.. 19th International Society for Magnetic Resonance in Medicine (ISMRM) conference; Montreal, Canada. 2011.
- Wedeen, V.; Dai, G. Diffusion-limited diffusion MRI and a universal optimum b-value.. 19th International Society for Magnetic Resonance in Medicine (ISMRM) conference; Montreal, Canada. 2011.
- Wedeen VJ, Hagmann P, et al. Mapping complex tissue architecture with diffusion spectrum magnetic resonance imaging. *Magn Reson Med*. 2005; 54(6):1377–1386. [PubMed: 16247738]
- Wedeen VJ, Wang RP, et al. Diffusion spectrum magnetic resonance imaging (DSI) tractography of crossing fibers. *Neuroimage*. 2008; 41(4):1267–1277. [PubMed: 18495497]
- Wiegell MR, Larsson HB, et al. Fiber crossing in human brain depicted with diffusion tensor MR imaging. *Radiology*. 2000; 217(3):897–903. [PubMed: 11110960]

- Wu YC, Alexander AL. Hybrid diffusion imaging. *Neuroimage*. 2007; 36(3):617–629. [PubMed: 17481920]
- Wu YC, Alexander AL. Hybrid diffusion imaging. *Neuroimage*. 2007; 36(3):617–629. [PubMed: 17481920]
- Yeh FC, Wedeen VJ, et al. Generalized q-sampling imaging. *IEEE Trans Med Imaging*. 2010; 29(9): 1626–1635. [PubMed: 20304721]
- Zalesky A, Fornito A, et al. Disrupted axonal fiber connectivity in schizophrenia. *Biol Psychiatry*. 2011; 69(1):80–89. [PubMed: 21035793]

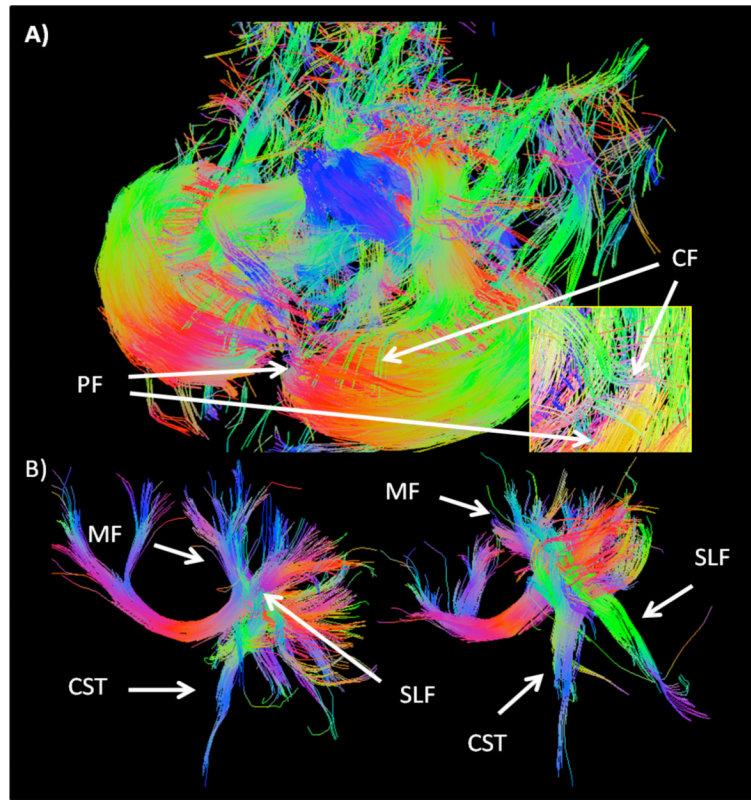


Figure 1. Fiber configuration of the cerebellum and its cortex (A) and of the corona radiata (B) showing 2 patterns of crossing fibers in the human brain. PF: parallel fibers; CF: climbing fibers; MF: motor fibers; CST: cortico-spinal tract; SLF: superior longitudinal fasciculus.

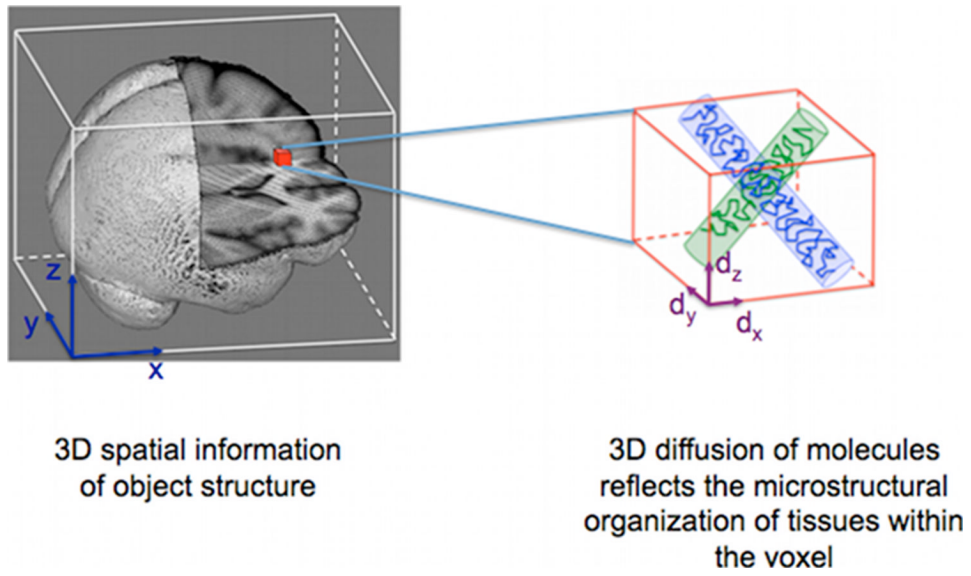


Figure 2. Diffusion imaging is a six-dimensional imaging technique, providing structural information at the image level (left panel) as well as the organization of the tissues (right panel) within each voxel.

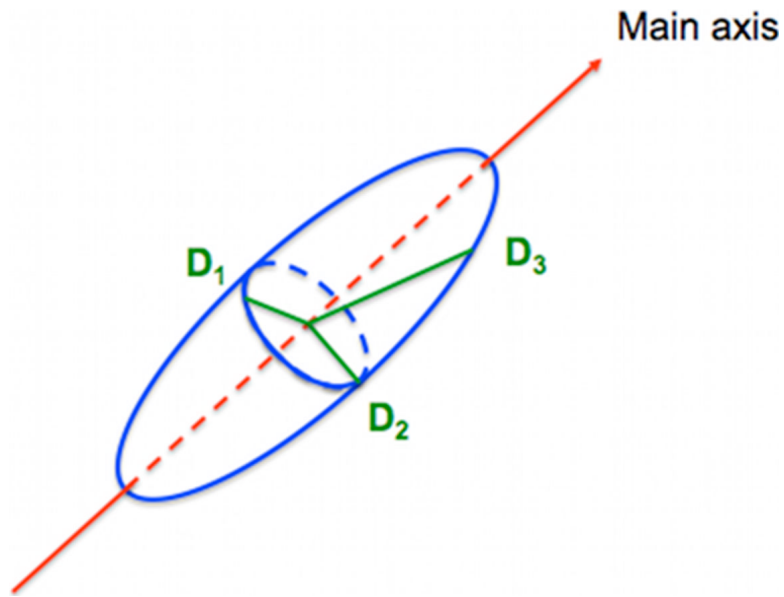


Figure 3. Three-dimensional ellipsoid assumption of ADC profile in a voxel. The blue line delineates the 3D ellipsoid, which demarks the ADC value for each possible diffusion encoding direction (defined through a line starting at the origin and ending at the particular point on the 3D surface). D_1 , D_2 , and D_3 are the ADC values in the respective directions.

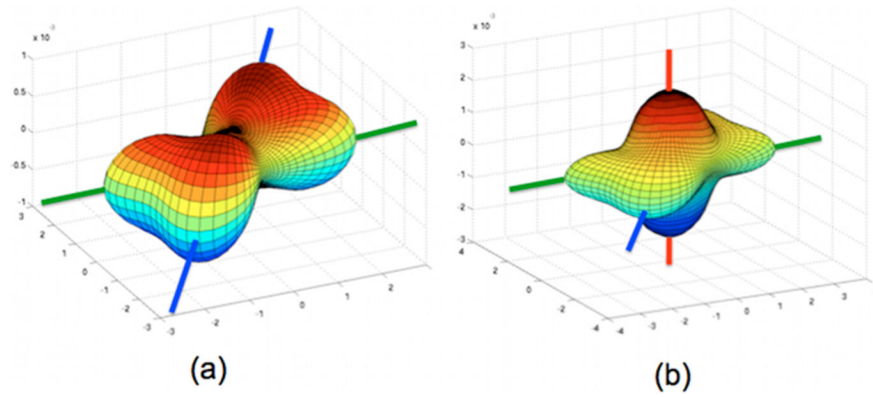


Figure 4. Simulation results show the ADC profiles of a voxel with: (a) two crossing fibers and (b) three crossing fibers. The underlying fiber orientations are also shown with solid lines (red, green, and blue). The colored 3D surface demarks the ADC value for each possible diffusion encoding direction (defined through a line starting at the origin and ending at the particular point on the 3D surface).

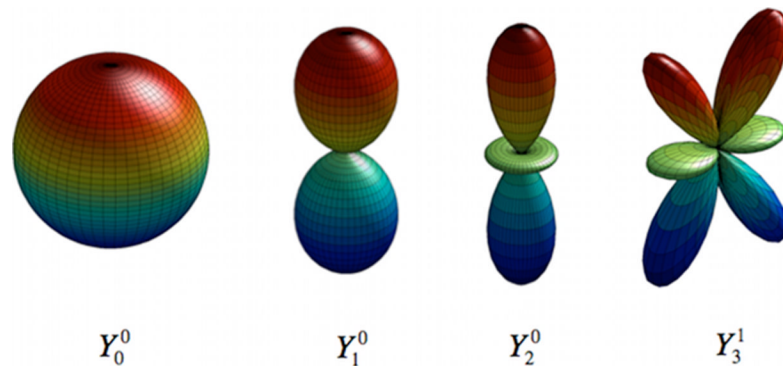


Figure 5. Illustrations of the real parts of spherical harmonics with different degrees and orders. Spherical harmonic of degree l and order m is denoted as Y_l^m .

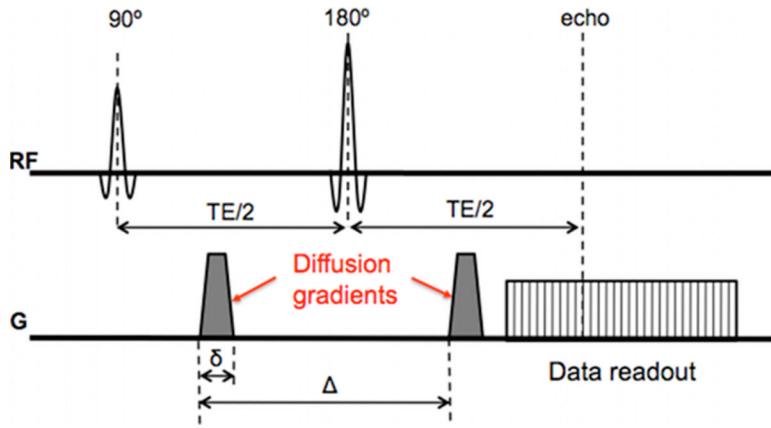


Figure 6. Diagram of a standard spin-echo diffusion-weighted pulse sequence for q-space imaging. Notice that the diffusion-encoding gradients are much shorter than those for conventional DWI.

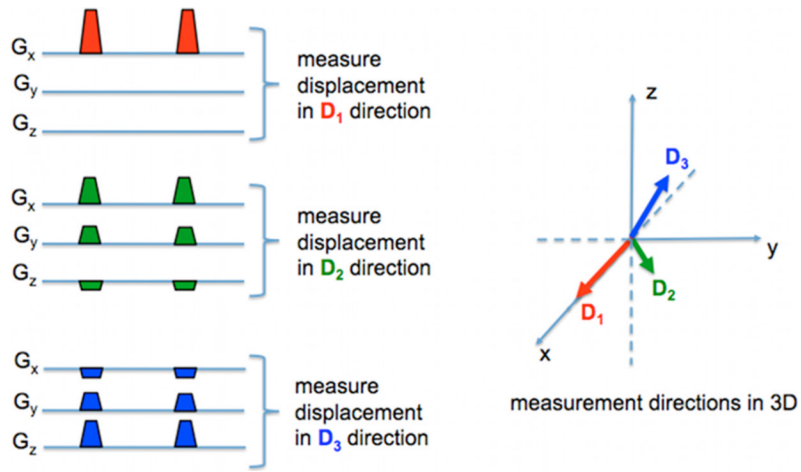


Figure 7. Adjustment of the displacement measurement direction by changing the heights of the diffusion-encoding gradients (shaded trapezoids) generated by combining the three gradient channels (G_x , G_y , and G_z). Examples of three gradient schemes are shown on the left with their corresponding displacement measurement directions in 3D on the right. The gradient strengths played out on each axis determine both the direction and magnitude of diffusion-sensitization.

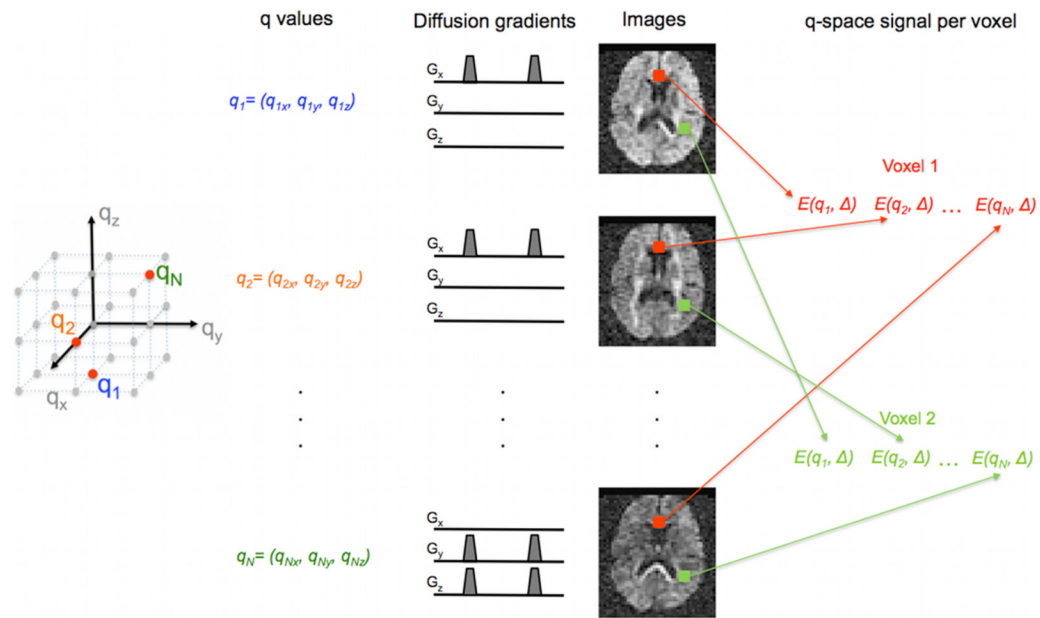


Figure 8. Acquisition of individual q-space signal samples at different locations in the brain. The q-space coordinate values are defined by the diffusion-encoding gradients applied on G_x , G_y , and G_z channels, the duration of the diffusion-encoding gradients, and the gyromagnetic ratio. Diffusion-weighted images are acquired with different diffusion encodings (q-values). The q-space signal, E , of a particular voxel is obtained by collecting the signal from those voxel in all of the diffusion-weighted images.

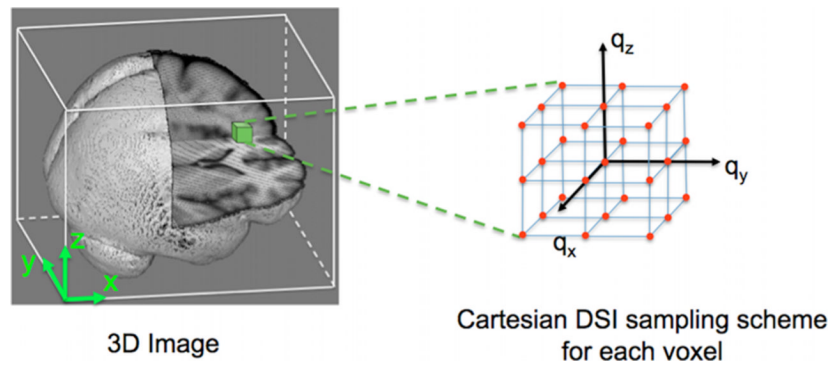


Figure 9. The 3D Cartesian sampling scheme of diffusion spectrum imaging for a single voxel. The red dots indicate the q -values used in the acquisition.

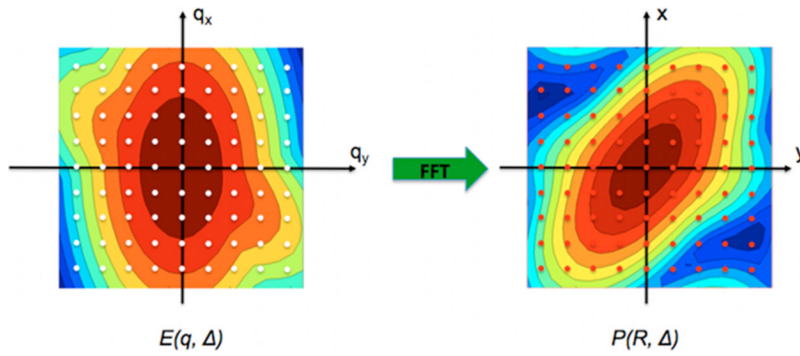


Figure 10.

A two-dimensional illustration of the procedure for estimating the displacement distribution or PDF, $P(R, \Delta)$, for a single voxel. The white dots show the q -space location at which a measurement is obtained. The values of $E(q, \Delta)$ at the white dot grid (discretized q -space) are 2D Fourier transformed (FFT) to give samples of the displacement distribution $P(R, \Delta)$ (again at discrete locations) on the red dot grid. Here, red is resembles a higher likelihood that a spin (originally at $[0,0]$ location) gets displaced to a position $[x,y]$ than turquoise or blue.

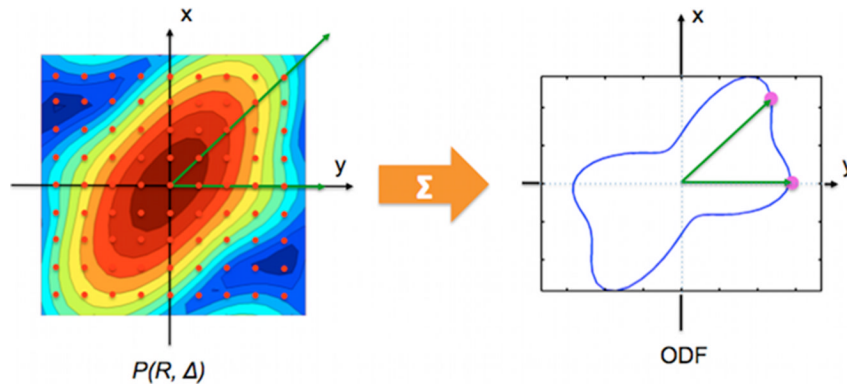


Figure 11. The values of the ODF (distances from the pink dots to the origin) in the directions pointed out by the green arrows (right panel) are the sum of the values (the red dots) of the displacement distribution $P(R, \Delta)$ on the corresponding green arrows on the left panel, weighted by square of their distances to the origin. The values of the ODF are computed at many directions and then interpolated to get the continuous ODF (blue lines).

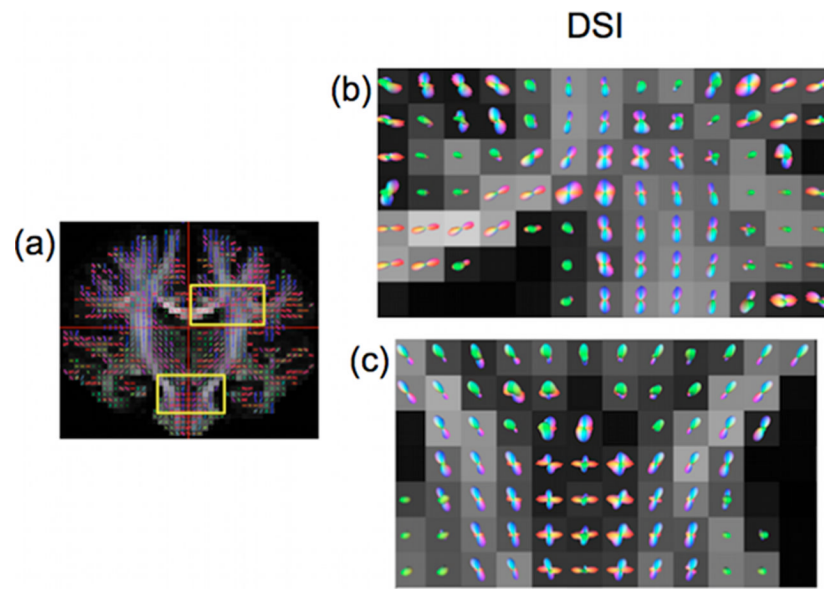
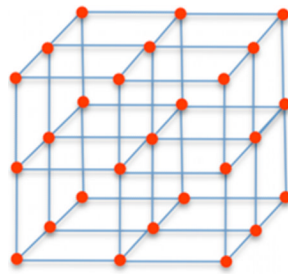
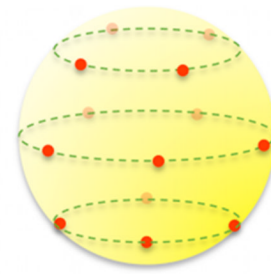


Figure 12. ODF maps of a region close to the corpus callosum (b) and the mid brain (marked by yellow boxes in (a)). Expected crossing fibers were detected from the shape of the ODFs.



DSI sampling



Q-ball sampling

Figure 13. Examples of sampling schemes used in DSI and q-ball imaging. The red dots indicate the sampling points in q-space. Notice that q-ball imaging samples only a sphere of radius q_b in q-space.

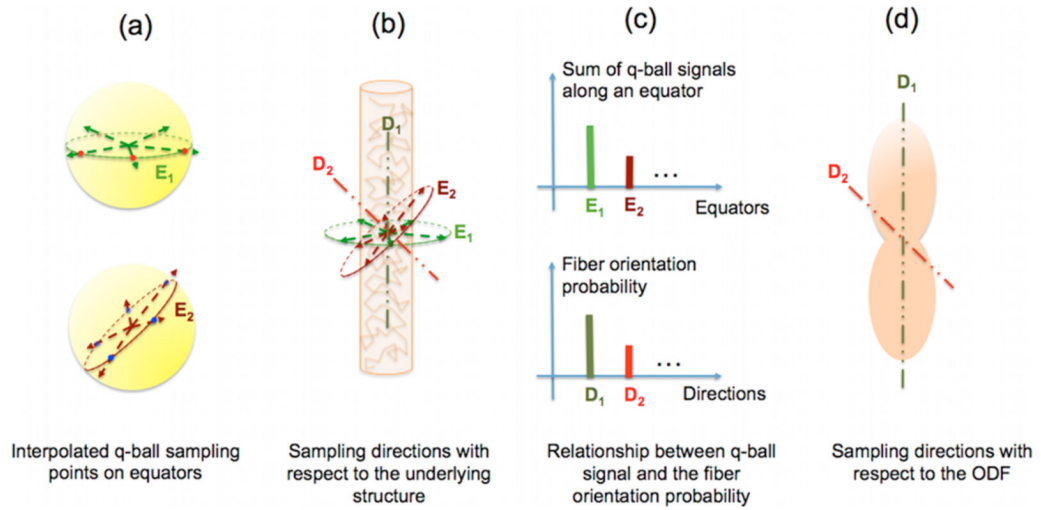


Figure 14.

Relationship between q-ball signal and the ODF: the sum of q-ball signal along an equator (for example E_1 , or E_2) is proportional to the probability that the fibers orient in the direction perpendicular to that equator. This is also called the Funk-Radon transform. The sum of the q-ball signal along E_1 or E_2 gives an estimation of the probability that the fibers are oriented along the direction D_1 or D_2 , respectively.

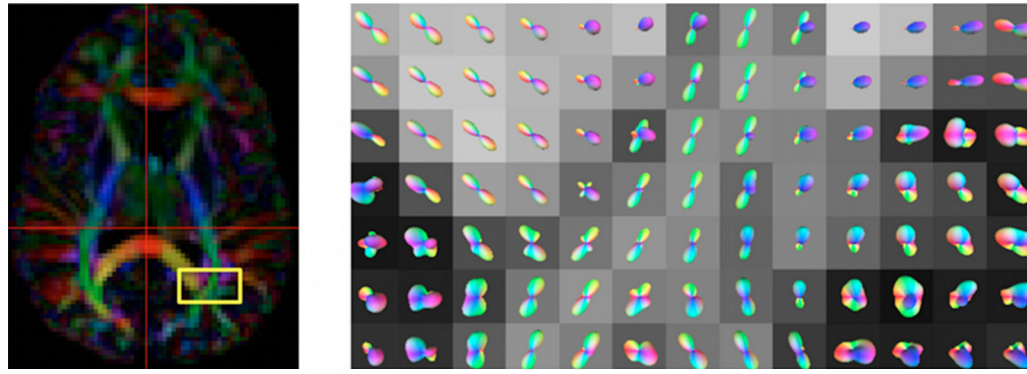


Figure 15. In vivo ODF maps (right panel) in a region of interest (marked by the yellow box overlaid on the corresponding color-coded FA maps on the left) obtained from a q-ball acquisition using the FRT transform.

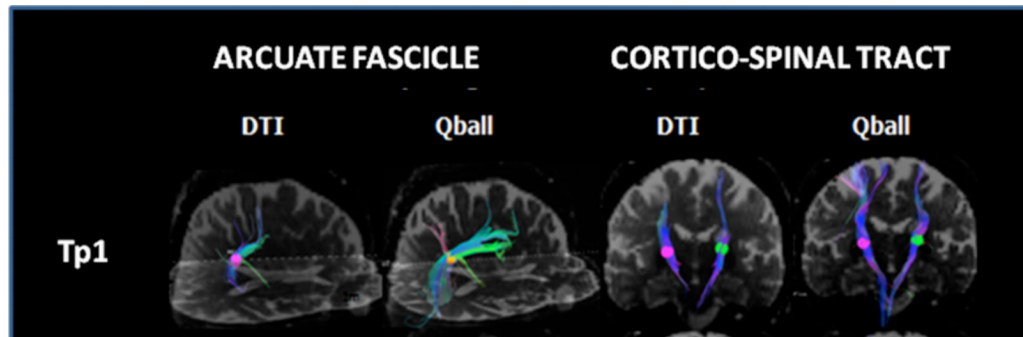


Figure 16.

DTI and q-ball tractography of the arcuate fasciculus (AF) and the cortico-spinal tract (CST) at 3 different time points after stroke (Tp1: acute phase; Tp2: 1 month after stroke; Tp3: 6 months after stroke). Spherical region of interest (ROIs) are located at the stroke periphery and the tract subserving the stroke lesion is shown. Q-ball tractography appears anatomically more accurate in showing the AF and the CST at different time points after stroke.

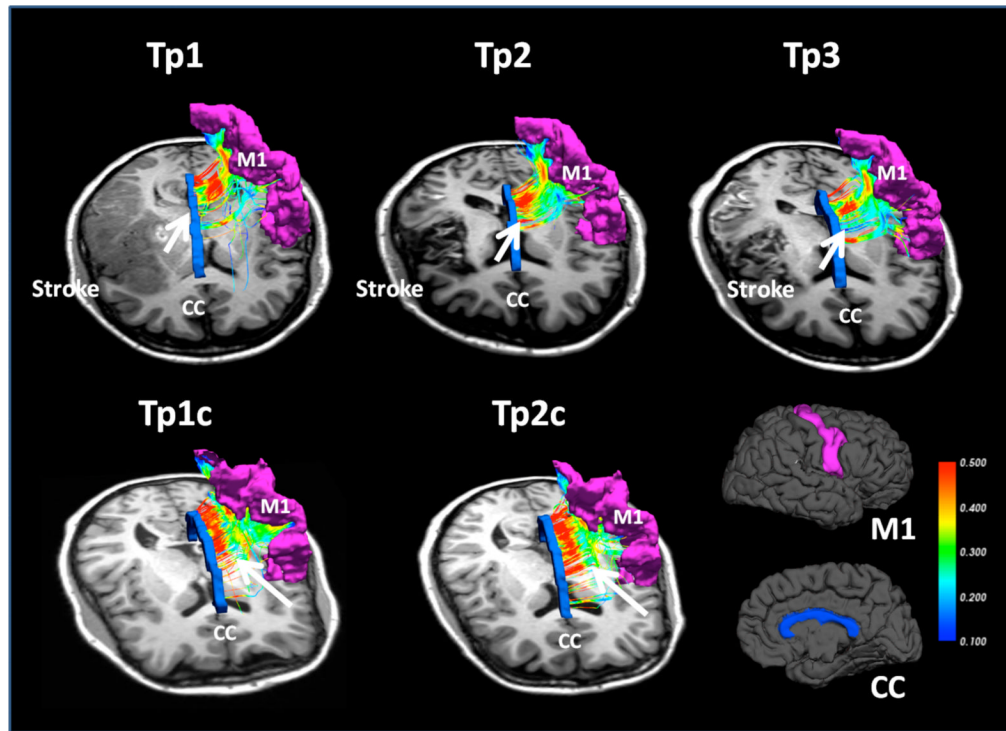


Figure 17.

DSI tractography view of the interhemispheric connections between the primary motor area (M1) and the corpus callosum (CC) in the contralateral healthy hemisphere of a stroke patient (top, tp1: acute MRI -tp2: MRI after one month and tp3: MRI after six months) and in one hemisphere of control subject (bottom, tp1 c and tp2c, MRI performed within one month interval). Fiber trajectories are color-coded using a scalar scale based on GFA (max value 0.5 and min value 0.1). In the control subject (lower row), arrows indicate the absence of substantial differences between the first and second time point, tp1c and tp2c, (one month interval); on the contrary, in the patient, arrows show a decrease in GFA between tp1 and tp2 and between tp2 and tp3.

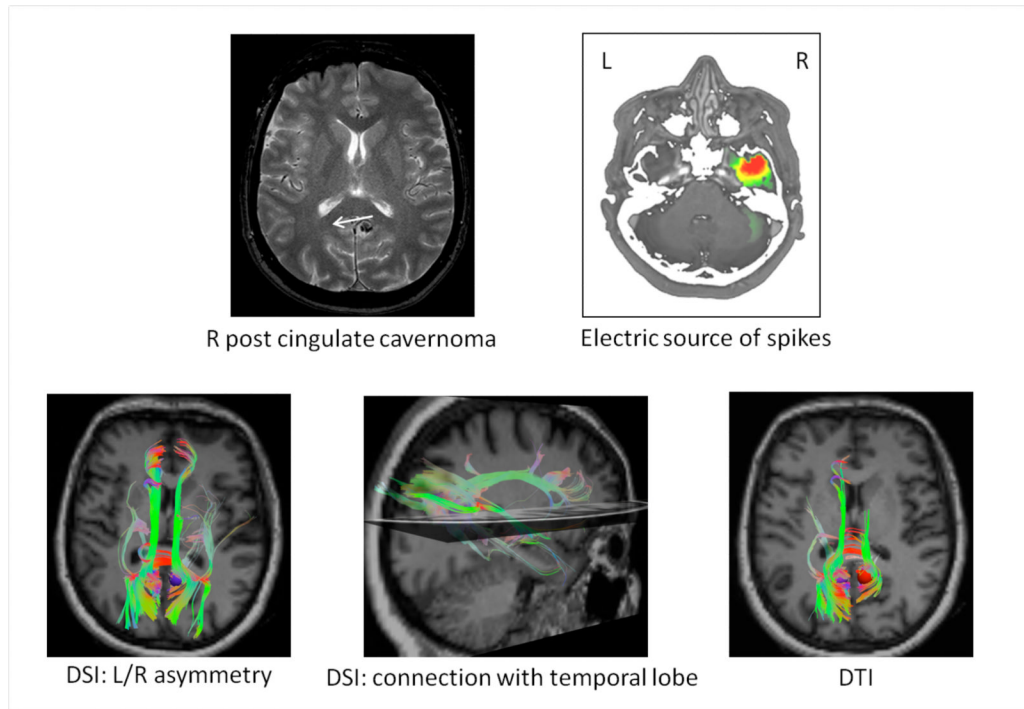


Figure 18.

Female patient, 51y, with medically refractory focal epilepsy symptomatic of a right posterior cingulate cavernoma (white arrow on T2 –weighted image, top left). EEG and electric source imaging showed right anterior temporal epileptic focus (top right). DSI seeded from the perilesional tissue identifies cingulate connections with the temporal lobe and shows globally reduced connectivity from the right posterior cingulate compared to the contralateral hemisphere (bottom left and middle). By contrast, the sensitivity of DTI was insufficient to map these connections (bottom right). Courtesy of A. Lemkaddem (EPFL, Lausanne, CH) and Dr S. Vulliemoz (Geneva University Hospital, Geneva, CH).

Table 1

Advantages and disadvantages of the presented diffusion imaging techniques.

Technique	Information Estimated in Each Voxel	Advantages	Disadvantages
Diffusion Tensor Imaging (DTI)	3D diffusion tensor	<ul style="list-style-type: none"> -Short acquisition time. -Provides information about diffusion orientation and anisotropy. - Not hardware demanding. - DTI metrics based on FA are validated and accepted. - Reproducibility studies are widely available 	<p>Hypothesis-based. Does not provide accurate information of complex fiber architecture. Tractography results are vulnerable to severe artifacts.</p>
Diffusion Spectrum Imaging (DSI)	3D diffusion displacement distribution	<ul style="list-style-type: none"> -Hypothesis-free. Provides accurate depiction of complex fiber architectures. -Maps the entire field of diffusion with possibility of many different characterizations of the imaged structures. 	<ul style="list-style-type: none"> -Relatively long acquisition time. Recent improvements in hardware and imaging techniques have made acquisition time shorter. -Demanding hardware requirements. -Lacking consensus on proper quantitative metric -Limited number of reproducibility studies
Q-ball Imaging	3D fiber orientation distribution	<p>Tolerable acquisition time. Provides information about diffusion orientation and anisotropy, depiction of fiber crossings.</p>	<ul style="list-style-type: none"> -Demanding hardware requirements. -Although results seem correct in important brain areas, accuracy is not guaranteed in all brain regions. Further validation of the technique required. -Lacking consensus on proper quantitative metric. -Limited number of reproducibility studies